ELSEVIER

Journal of Alloys and Compounds 404–406 (2005) 112–117

Journal of ALLOYS AND COMPOUNDS

www.elsevier.com/locate/jallcom

Hydrogen assisted order–disorder transformations in Cu–Sn sublattices of the (La,Ce)CuSn–D_2 systems

J.P. Maehlen[a], M. Stange[a], V.A. Yartys[a,*], R.G. Delaplane[b]

[a] *Institute for Energy Technology, P.O. Box 40, NO-2027 Kjeller, Norway*
[b] *The Studsvik Neutron Research Laboratory, Uppsala University, S-611 82 Nyköping, Sweden*

Received 6 September 2004; accepted 25 September 2004
Available online 1 August 2005

Abstract

The equiatomic RTX intermetallic compounds (R = rare earth metal; T = Fe, Co, Ni; X = non-transition element) exhibit interesting crystal structures, hydrogenation and magnetic properties. The hexagonal intermetallics are frequently formed in these systems and can be obtained via internal and external deformation of the AlB_2-type metal sublattice accompanied by a partial substitution of T by X. This work was focused on studies of hydrogen interaction with LaCuSn and CeCuSn intermetallics. Original compounds crystallise with the hexagonal "a*2c" type structures characterised by ordering of Cu and Sn with a slight internal deformation. $(c/a)_{hex}$ was found to be significantly higher for R = La. The structural phase transformations were studied by synchrotron XRD and powder neutron diffraction. The hydrogenation is accompanied by a small volume expansion (0.8–1.1%) proceeding exclusively along [0 0 1] and leading to a rebuilding of the structures of (La,Ce)CuSn$D_{0.3–0.5}$ into deformed AlB_2 type (Cu + Sn disordered; "a*c" cells). Deuterium atoms partially occupy trigonal bipyramidal R_3Sn_2 sites with D slightly shifted from the R_3 planes towards the R_3Sn tetrahedra. Thermal desorption properties studied by the vacuum TDS technique show that D desorption leads to a reversible formation of the initial intermetallics that restores the LiGaGe (Cu + Sn ordered) type structure.

Keywords: Intermetallics; Interstitial alloys; X-ray diffraction; Neutron diffraction

1. Introduction

The equiatomic RTX intermetallic compounds (R= rare earth metal; T= Fe, Co, Ni, Cu; X= non-transition element) exhibit interesting crystal structures [1–3], magnetic and hydrogenation properties [4–6]. In the present work, hydrogenation properties of two related RTX intermetallics, LaCuSn and CeCuSn are studied. Main attention has been to establish the hydrogen–tin environments. The motivation for this is two-fold: in previous work on the related LaNiSn– and CeNiSn–H systems [5,6] it was shown that H storage capacity reaches 2 at. H/fu in maximum with a formation of the ZrBeSi-type related hydrides. Interestingly, for the H–$LaNi_3$ sites in LaNiSn–H, when tin partially and slightly substituted Ni, H-blocking in the formed La_3(Ni,Sn) interstices did not take place. Thus, the influence of tin on the hydrogenation properties seemed to be different from the typical 'blocking' behaviour characteristic for non-metals. Another factor that has motivated the present work is the special effects Sn substitution plays in the AB_5-type of metal hydrides. For the $LaNi_5$–H system, it has been shown that Sn, when introduced as a partial substituting metal for Ni, can play a beneficial role increasing charging-discharging cycling stability [7].

The hexagonal intermetallics are frequently formed in the RTX systems and can be obtained via external and internal deformation of the AlB_2-type metal sublattice accompanied by an ordered or disordered distribution of T and X [2,3]. The structures can be visualised as a stacking of alternating layers of rare earth trigonal nets (A) and T–X honeycomb nets (H) in the sequence AHAH'AH", etc. (see Fig. 1).

This work was focused on studies of hydrogen interaction with LaCuSn and CeCuSn intermetallics. Structural work was performed using synchrotron powder X-ray diffraction (SRPXD) and powder neutron diffraction (PND). Hydrogen

* Corresponding author. Tel.: +47 63 80 64 53; fax: +47 63 81 29 05.
E-mail address: volodymyr.yartys@ife.no (V.A. Yartys).

0925-8388/$ – see front matter © 2005 Elsevier B.V. All rights reserved.
doi:10.1016/j.jallcom.2004.09.086

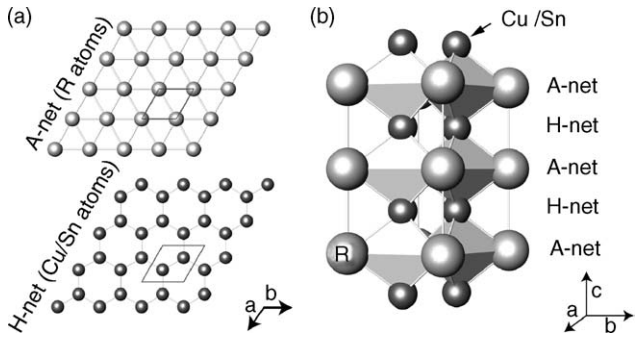

Fig. 1. Description of the AlB_2 type related structures showing (a) the rare earth trigonal nets (A) and T (Cu)–X (Sn) honeycomb nets (H), and (b) the generated structures by alternating stacking of the nets along the *c*-axis creating corner-shearing $R_3(T/X)_2$ trigonal bipyramidals. Structures with AHA . . . stacking (generated by only two nets) will be called '*a***c*'-type structures, while structure with AHAH' . . . will be labelled '*a**2*c*'-type structures, etc.

desorption properties were investigated using thermal desorption spectroscopy (TDS).

2. Experimental part

2.1. Synthesis

The alloys CeCuSn and LaCuSn were prepared by arc melting in argon atmosphere (Ce, La, Cu, Sn > 99.9%). The ingots were remelted several times to increase their homogeneity and, after cooling, subjected to annealing treatments. The quality of the samples was confirmed by laboratory powder X-ray diffraction.

To reduce incoherent scattering contribution during the PND experiments, a deuterium (purity 99.8%) loaded sample was used instead of hydrogen. After activating the sample in vacuum, the deuterium loading (deuteration) was performed by the direct gas–solid state reaction where the samples were kept for 1 h in ∼4 bar D_2 atmosphere at ∼700 K and subsequently cooled down to room temperature. TDS was performed under secondary vacuum condition (vacuum in the range 2×10^{-5} to 7×10^{-3} mbar).

2.2. Characterisation

Laboratory powder X-ray diffraction data were collected with a Siemens D5000 diffractometer equipped with a Ge primary monochromator giving Cu $K\alpha_1$ radiation. SRPXD data were collected at the Swiss-Norwegian Beam Line (BM01B) at ESRF, Grenoble, France (Si(1 1 1) channel-cut monochromator, $\lambda = 0.50000$ Å, scintillation detectors). Powder neutron diffraction data of the deuterides was collected at the R2 reactor at The Studsvik Neutron Research Laboratory (NFL), Studsvik, Sweden, with use of the high-resolution NPD instrument [a double Cu (2 2 0) monochromator; $\lambda =$ 1.470 Å, 2θ-range = 1.2–137°, $\Delta 2\theta = 0.08°$, $35\,^3$He detectors, $T = 293$ K]. The sample was contained in a vanadium sample holder sealed with an indium washer to prevent contact with air.

All the powder diffraction data were analysed according to the Rietveld-type method [8] using the General Structure Analysis System (GSAS) software [9]. Adopted scattering lengths for the elements were taken from the library of the program. Combined Rietveld analysis were performed for the PND and SRPXD data of the deuterides.

Details concerning the collected diffraction data and crystallographic structure data are given in Table 1.

Table 1
Crystal structure data (unit cell parameters and summary of the diffraction data (∼295 K) derived from Rietveld refinements of powder diffraction data for CeCuSn, $CeCuSnD_{0.33}$, LaCuSn, and $LaCuSnD_{0.47}$)

	CeCuSn	$CeCuSnD_{0.33(2)}$	LaCuSn	$LaCuSnD_{0.47(5)}$
Space group	$P6_3mc$	$P3m1$	$P6_3mc$[a]	$P3m1$
a (Å)	4.58537(1)	4.53244(5)	4.5808(1)	4.54106(6)
Δa (%)[b]	–	−1.15	–	−0.87
c(Å)	7.8576(1)	4.0660(1)	8.1693(3)	4.19101(9)
Δc (%)[b]	–	3.49	–	2.60
V (Å^3)	143.077(3)	72.337(2)	148.458(6)	74.845(2)
Z	2	1	2	1
$\Delta V/V$ (%)[b]	–	1.12	–	0.83
Specific volume[c]	23.85	24.11	24.74	24.95
Data collection	SRPXD	SRPXD/PND	SRPXD	SRPXD/PND
Wavelength (Å)	0.5	0.5/1.47	0.5	0.5/1.47
Angle range (2θ)	5–25	3–34/4–140	5–25	2–35/4–140
Step lengths ($\Delta 2\theta$)	0.008	0.005/0.8	0.008	0.005/0.8
R_p (%)	4.09	6.38[d]	4.89	10.53[d]
Rw_p (%)	5.84	14.1 [d]	8.02	14.83[d]

Calculated standard deviations in parenthesis.

[a] LaCuSn can also be fitted using centro symmetric space group $P6_3/mmc$.
[b] Compared to the respective value for the initial alloy.
[c] Specific volume defined as V_{cell}/N, where N is the number of metal atoms in the cell ($N = 6$ for the alloys, $N = 3$ for the deuterides).
[d] Combined Rietveld refinements of SRPXD and PND data.

3. Results and discussion

3.1. The initial alloy

For both CeCuSn and LaCuSn, some small R-containing impurities were present. After completing a hydrogenation – dehydrogenation cycle, it was observed that the relative intensity of the impurity reflections compared to the (Ce,La)CuSn reflections increased.

From SRPXD measurements it was found that both CeCuSn and LaCuSn crystallise in the "a*2c" type structures with a layer packing sequence of AHAH'A ... characterised by ordering of Cu and Sn. For both CeCuSn and LaCuSn the LiGaGe-type structure (space group $P6_3mc$, $a = 4.58537(1)$, $c = 7.8576(1)$ Å for CeCuSn and $a = 4.5808(1)$, $c = 8.1693(3)$ Å for LaCuSn) gave the best fits to the experimental data. Details concerning the collected diffraction data and unit cell dimensions are given in Table 2. Atomic coordinates, temperature factors and fractional occupation numbers are reproduced in Table 3. Example of a Rietveld type fit of the SRPXD data (LaCuSn) is given in Fig. 2. The $(c/a)_{hex}$ for R= La is significantly higher than for R= Ce; $(c/a)_{hex} = 0.892$ and $(c/a)_{hex} = 0.857$, respectively.

The possibility for partial disorder in the Cu–Sn sublattice was explored by refining cells with mixed occupations in the 2b positions (see Table 3). A model of 10 % disorder in the Sn–Cu sublattice (one site contains 10 at.% Cu and 90 at.% Sn, while the other site contains 90 at.% Sn and 10 at.% Cu) gave the best fit. From reference data, Sn(III) has a radius of 1.623 Å in intermetallic compounds, while Sn(IV) has a radius of 1.545 Å [10]. The latter radius is closer to the Cu radius (1.278 Å), and thus Sn(IV) is more likely to be randomly substituted by Cu atoms. This may indicate a statistical distribution of Sn(III)–Sn(IV) in the structure. It

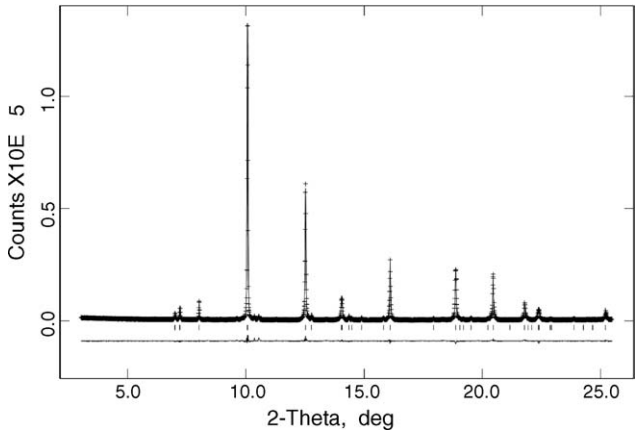

Fig. 2. Rietveld type plots of SRPXD pattern for LaCuSn showing observed (crosses), calculated (upper line), and difference (bottom line) plots. The positions of the Bragg peaks are shown as ticks.

Table 2
Crystal structure data (atomic coordinates[a], occupation (n) and isotropic temperature factors ($U_{iso} \times 100$ Å^2)) as derived from Rietveld refinements of SRPXD data for CeCuSn and LaCuSn, and combined Rietveld refinements of SRPXD and PND data for $CeCuSnD_{0.33(2)}$ and $LaCuSnD_{0.47(5)}$

Atom		Site	CeCuSn	Site	$CeCuSnD_{0.33}$	Site	LaCuSn	Site	$LaCuSnD_{0.47}$
R[b]	U_{iso}	2a	0.81(4)	1a	1.06(8)	2a	0.71(4)	1a	0.97(3)
	n		1[c]		0.959(5)		1[c]		1[c]
	z		0.25[c]		0[c]		0.25[c]		0[c]
Cu	U_{iso}	2b1	1.03(8)	1b	1.05(6)	2b1	0.84(4)	1b	0.67(5)
	n		0.91(1)[d]		0.57(1)		0.890(5)[d]		0.5[c]
	z		0.026(4)[e]		0.517(4)		0.007(1)[e]		0.441(1)
Cu	U_{iso}	2b2	1.03(8)	1c	1.05(6)	2b2	0.84(4)	1c	0.67(5)
	n		0.1(1)[d]		0.43(1)		0.101(5)[d]		0.5[c]
	z		−0.017(4)[e]		0.626(5)		−0.004(1)[e]		0.583(1)
Sn	U_{iso}	2b1	1.03(8)	1b	1.05(6)	2b1	0.84(4)	1b	0.67(5)
	n		0.91(1)[d]		0.43(1)		0.110(5)[d]		0.5[c]
	z		0.026(4)[e]		0.474(4)		0.007(1)[e]		0.523(1)
Sn	U_{iso}	2b2	1.03(8)	1c	1.05(6)	2b2	0.84(4)	1c	0.67(5)
	n		0.09(1)[d]		0.52(1)		0.899(5)[d]		0.5[c]
	z		−0.017(4)[e]		0.475(5)		−0.004(1)[e]		0.477(1)
D	U_{iso}	–		1c	0.5(6)	–		1c	2(1)
	n				0.33(2)				0.47(5)
	z				0.959(8)				0.96(3)

Calculated standard deviations in parenthesis.

[a] Occupied positions are for LaCuSn (space group $P6_3/mmc$): 2a (0, 0, 0), 2c (1/3, 2/3, 1/4), 2d (2/3, 1/3, 3/4); for CeCuSn (space group $P6_3mc$): 2a (0, 0, z), 2b1 (1/3, 2/3, z), 2b2 (2/3, 1/3, z); for $RCuSnD_x$ (R= Ce or La, space group $P3m1$): 1a (0, 0, z), 1b (1/3, 2/3, z), 1c (2/3, 1/3, z).

[b] R = Ce or La.

[c] Fixed.

[d] n in same site constrained such that $\sum n = 1$.

[e] z for atoms in same site constrained to be equal.

Table 3
Estimations of the amount of Sn–Cu ordering in the alloy CeCuSn (LiGaGe-type structure, space group $P6_3mc$) by Rietveld refining of SRPXD data using different starting configurations for the two 2b sites occupied by Sn/Cu (atomic z-coordinates (z), occupation (n) and isotropic temperature factors ($U_{iso} \times 100$ Å^2)

Site 2b1 (1/3, 2/3, z)		Site 2b2 (2/3, 1/3, z)		Goodness of fit			Notes
n Sn	n Cu	n Sn	n Cu	χ^2	R_p (%)	wR_p (%)	
0	1	1	0	9.9	5.2	7.2	A
0.1	0.9	0.9	0.1	8.4	4.3	5.8	A
0.2	0.8	0.8	0.2	9.7	4.9	6.9	A
0.3	0.7	0.7	0.3	12.1	5.5	8.7	A
0.4	0.6	0.6	0.4	14.1	5.9	9.9	A
0.5	0.5	0.5	0.5	14.9	6.1	10.3	A
0.09	0.91	0.097	0.90	8.4	4.3	5.8	B

A, Constraints: same U_{iso} and position for both atoms in same site. Refined on U_{iso} and z. B, Constraints: same U_{iso} and position for both atoms in same site. Refined on U_{iso}, n and z

should also be noted that from refining the atomic fractions for completely ordered cells, it was found an improvement of the fits for both alloys if allowing the Ce/La and Sn content to be lower than unity (i.e. $Ce_{0.924(8)}CuSn_{0.886(8)}$ and $La_{0.920(6)}CuSn_{0.875(6)}$). Both models, the 10% disordered model and the completely ordered model with excess of Cu, gave approximately the same goodness of fit. The rather large Cu over-stochiometry for the latter model seems unreasonable. In addition, diffraction studies of NdCuSn by Pacheco et al. [11,12] also revealed a partial disordered Cu–Sn sublattice (10% disordered).

From the literature [2], CeCuSn should form a $CaIn_2$-type structure, while LaCuSn should form a "a*c" AlB_2-type structure, both with disordered Cu + Sn. The results obtained in this work do not confirm those findings. SRPXD investigation of the alloys after completing a hydrogenation–dehydrogenation cycle showed that the alloys reverted to their initial "ordered" crystal structures.

3.2. Deuterides

The two deuterides $CeCuSnD_x$ ($x = 0.5 \pm 0.1$) and $LaCuSnD_x$ ($x = 0.7 \pm 0.1$) were prepared as described in the experimental part. The deuterium content given in the formulas above was estimated from the volumetric measurements. Crystal structure data for the deuterides are given in Tables 1 and 2. The ordering of Sn and Cu found for the initial alloys is not observed for the deuterides. From SRPXD of both deuterides, best fits were obtained using "a*c" type of structures. The structure is built up by corner-sharing $R_3(Cu/Sn)_2$ bipyramids. During hydrogenation, a small volume expansion is observed (0.8% for R= La, 1.1% for R= Ce) proceeding exclusively along [0 0 1].

Choosing the AlB_2 structure type, no discrimination can be made between R_3Sn_2 and R_3Cu_2 sites, and therefore lower symmetry groups were tested. Using space group $P3\,m1$, a Cu/Sn disordered structure can be represented by allowing both the two honeycomb-net generating positions to be occupied by 50% Cu and 50% Sn. Anisotropic temperature factors were refined showing a considerable expansion of the anisotropic thermal ellipsoids along the c-axis for these positions, indicating the possibility for non-similar positions (z-coordinates) for Cu compared to Sn in the same crystallographic site. Thus, refinements on z and occupation numbers of both the Cu and Sn atoms were performed. By performing a combined Rietveld analysis of SRPXD data and PND data, it was found that deuterium only occupies one out of two possible $R_3(Cu/Sn)_2$ sites. Refining the z-position of the deuterium atom showed that the atom is not located in the centre of the bipyramidal but shifted slightly along the c-axis towards one of the Sn/Cu positions ($\delta z = 0.18$ Å).

For both deuterides, relatively broad extra reflections were observed in the diffraction patterns. These reflections are not present in the alloys after completing a hydrogenation–dehydrogenation cycle. No reasonable superstructures were found that could explain these reflections. The D contents of the samples as estimated from the Rietveld refinements are somewhat lower than the volumetric estimations. The presence of an unknown additional hydride (R-containing) as a result of a disproportionation effect can explain the presence of both the extra reflections, and the lower D content of the (La/Ce)$CuSnD_x$ deuterides. The individual atomic coordinates for $CeCuSnD_{0.33(2)}$ and $LaCuSnD_{47(5)}$ are given in Table 2, while selected interatomic distances are given in Table 4. The combined Rietveld type fit of the SRPXD and PND data of $CeCuSnD_{0.33(2)}$ is shown in Fig. 3.

To get some more information about the neighbourhood of the deuterium atoms, the interatomic distances to all its possible surrounding atoms were calculated (Table 5). For $CeCuSnD_{0.33(2)}$, assuming that the D site is located inside Ce_3Cu_2 or Ce_3CuSn bipyramidals, results in D–Cu interatomic distances of 1.45 Å and/or 2.60 Å. The first distance is unreasonably short (Cu radius is 1.28 Å, while typical radius for D is $R_D \geq 0.4$ Å), while the last results in a Cu atom that lies outside the immediate neighbourhood of the deuterium atom. Assuming the other possibility, that the D site is inside a Ce_3Sn_2 bipyramidal, gives D–Sn interatomic distances of 2.11 and 1.95 Å, both distances within what one would expect. The latter distance indicates that D prefers neighbourhood of Sn(IV) ($R_{Sn(III)} = 1.62$ Å, $R_{Sn(IV)} = 1.55$ Å). An illustration of the possible D-sites is given in Fig. 4. For the $LaCuSnD_{0.47}$ deuteride, the shorter D–Cu inter-

Table 4
Selected interatomic distances (Å) in CeCuSn, $CeCuSnD_{0.33}$, LaCuSn and $LaCuSnD_{0.47}$

Atoms	CeCuSn[b]	$CeCuSnD_{0.33}$	LaCuSn[b]	$LaCuSnD_{0.47}$
R–R[a]	3.92879(7)	4.0660(1)	4.0846(1)	4.19101(9)
R–Sn	3.22(2) – 3.38(2)	3.27(1)–3.41(1)	3.32196(6)–3.36126(6)	3.296(4)–3.418(4)
R–Cu	3.18(2) – 3.42(2)	3.03(1)–3.38(1)	3.306(5)–3.377(5)	3.15109(3)–3.51613(4)
Sn–Sn	–	2.6180(5)[c]	–	2.6291(9)[c]
Cu–Cu	–	2.649(2)[c]	–	2.68843(3)[c]
Sn–Cu	2.6685(5)–3.594(4)	2.629(2)–2.681(3)	2.64628(3)–3.995(5)	2.6260(4)–2.6336(6)

Calculated standard deviations in parenthesis.

[a] R = Ce or La.

[b] Interatomic distance to R for the 90% occupied Sn/Cu site.

[c] 'Artificial' interatomic distance due to the mixed Sn/Cu occupancy.

atomic distance is somewhat larger (D–Cu = 1.59 Å), but still suspiciously short (assuming D–Cu = $R_{Cu} + R_D$ this gives $R_D = 0.31\,Å < 0.4\,Å$). Thus, it seems reasonable to conclude that the deuterium atoms prefers R_3Sn_2-bipyramidals and avoids neighbourhood of Cu.

3.3. Thermal desorption spectroscopy

Several TDS experiments were performed on both samples. Typically, the TDS patterns showed two peaks, one at relatively low temperatures (T_{low}) and one at higher temperatures (T_{high}). However, a large discrepancy in the desorption temperatures were observed between the different TDS experiments, ranging from 350 to 570 K for T_{low}, and from 440 to 760 K for T_{high}. From the measurements, it seemed likely that the (La, Ce)CuSn system also could form lower deuterides. However, SRPXD data of samples prepared by heating the respective deuterides in vacuum up to 570 K did not reveal new diffraction features corresponding to a presence of lower deuterides. To investigate this further and to reveal whether the samples undergo some sort of disproportionation process, a $LaCuSnD_{0.5}$ sample was prepared (D content estimated by the volumetric method). The sample was then divided into two parts, where one was immediately tested by TDS, while the other was tested by TDS after first keeping it under D_2 pressure at 873 K for

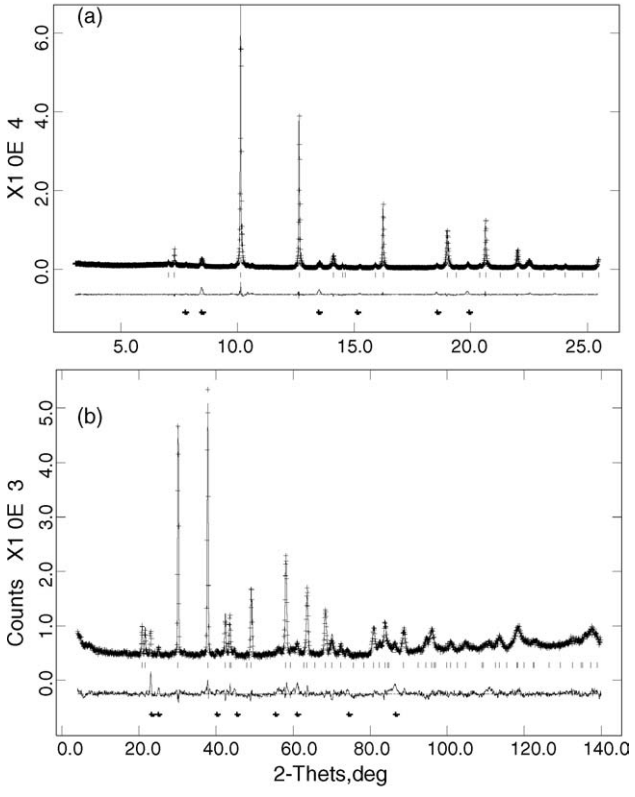

Fig. 3. Plots of the combined Rietveld type refinement of (a) SRPXD and (b) PND patterns for $CeCuSnD_{0.33(2)}$ showing observed (crosses), calculated (upper line), and difference (bottom line) plots. The positions of the Bragg peaks are shown as ticks. Un-indexed broad reflections attributed to non identified additional hydride are marked with asterisks.

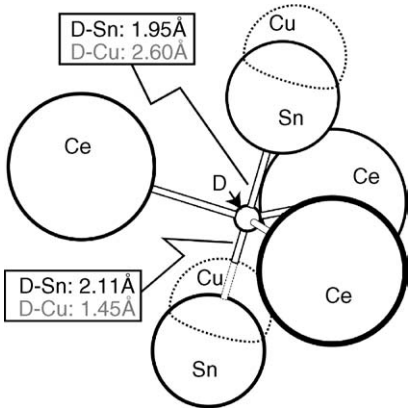

Fig. 4. Trigonal bipyramidal D-sites in $CeCuSnD_{0.33}$ as observed from the combined Rietveld type refinements of SRPXD and PND data assuming space group $P3m1$ and mixed Cu–Sn occupation.

Table 5
Calculated deuterium–metal interatomic distances (Å) in the $P3m1$ model of the deuterides $CeCuSnD_{0.33}$, and $LaCuSnD_{0.47}$

Atoms	$CeCuSnD_{0.33}$	$LaCuSnD_{0.47}$
D–R	2.618(1)	2.62657(3)
D–Cu 1	1.45(3)	1.58950(3)
D–Cu 2	2.60(3)	2.60214(3)
D–Sn 1	2.11(4)	2.156(6)
D–Sn 2	1.95(4)	2.035(6)

Calculated standard deviations in parenthesis. R = Ce or La.

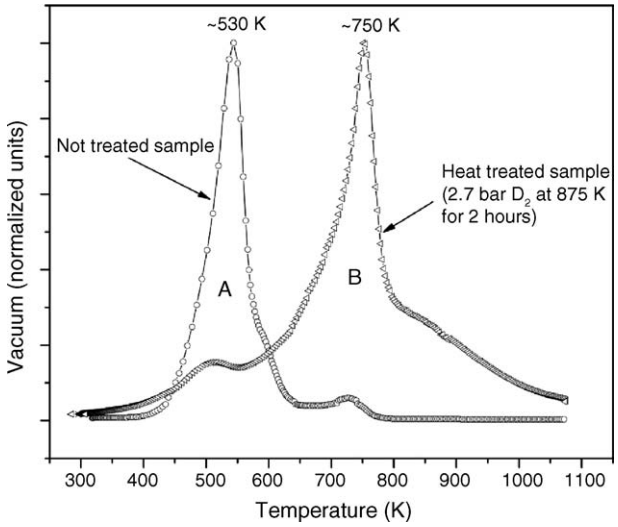

Fig. 5. Deuterium desorption traces from $LaCuSnD_{0.5}$ as prepared (A) and heat-treated in D_2-atmosphere (B) under dynamical vacuum conditions (heating rate 5 K/min).

2 h. As can be seen from the TDS plots of the two experiments (Fig. 5), the treatment induced a significant reduction of the low temperature deuterium traces and corresponding increase of the high temperature traces. This result gives evidence that disproportionation occurs in the system at elevated temperatures.

4. Conclusions

By high-resolution powder diffraction measurements it was shown that the (La, Ce) CuSn–D system undergoes a transition from a "a*2c" superstructure of the AlB_2-type structure where Cu/Sn are 90% ordered, to a Cu/Sn disordered state during hydrogenation. After removing the hydrogen at temperatures above 800 K, the Cu/Sn ordering reappears. In the deuteride phase, D atoms tend to favour R_3Sn_2 bipyramidal sites, avoiding close contact with Cu atoms. From TDS experiments and SRPXD data it is proposed that a disproportionation process occurs at elevated temperatures.

Acknowledgments

This work received funding from the Norwegian Research Council. We are also grateful to the Swiss Norwegian Beam Line at ESRF for the possibility to collect high quality diffraction data.

References

[1] P. Riani, et al., J. Phase. Equilib. 19 (1998) 239–251.
[2] R.V. Skolozdra, in: K.A.J. Gschneider, L. Eyring (Eds.), Handbook on the Physics and Chemistry of Rare Earths, Elsevier Science B.V., 1997.
[3] A. Szytuła, Crystal Structures and Magnetic Properties of RTX Rare Earth Intermetallics, Jagiellonian University Press, Krakow, 1988.
[4] V.A. Yartys, T. Olavesen, B.C. Hauback, H. Fjellvag, J. Alloy. Compd. 336 (2002) 181–186.
[5] V.A. Yartys, T. Olavesen, B.C. Hauback, H. Fjellvag, H.W. Brinks, J. Alloy. Compd. 330 (2002) 141–145.
[6] V.A. Yartys, B. Ouladdiaf, O. Isnard, O.Y. Khyzhun, K.H.J. Buschow, J. Alloy. Compd. 359 (2003) 62–65.
[7] R.C. Bowman, C.A. Lindensmith, S. Luo, T.B. Flanagan, T. Vogt, J. Alloy. Compd. 330 (2002) 271–275.
[8] H.M. Rietveld, J. Appl. Cryst. 2 (1969) 65–71.
[9] A.C. Larson, R.B.v. Dreele, General Structure Analysis System, LANL, Los Alamos, 1994.
[10] W.B. Pearson, The Crystal Chemistry and Physics of Metals and Alloys, Wiley, New York, 1972.
[11] J.V. Pacheco, K. Yvon, E. Gratz, Z. Kristallogr. 213 (1998) 510–512.
[12] J.V. Pacheco, K. Yvon, E. Gratz, P. Schobinger-Papamantellos, J. Phys. -Condens. Mat. 11 (1999) 4135–4141.